Nano Energy (2013) 2, 40–48

Available online at www.sciencedirect.com

SciVerse ScienceDirect

journal homepage: www.elsevier.com/locate/nanoenergy

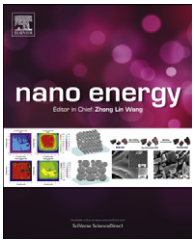

RAPID COMMUNICATION

# ZnO nanocrystallite aggregates synthesized through interface precipitation for dye-sensitized solar cells

Rui Gao[a,b], Zhiqiang Liang[a], Jianjun Tian[a], Qifeng Zhang[a], Liduo Wang[b,*], Guozhong Cao[a,*]

[a]*Department of Materials Science and Engineering, University of Washington, Seattle, WA 98195, USA*
[b]*Key Lab of Organic Optoelectronics & Molecular Engineering of Ministry of Education, Department of Chemistry, Tsinghua University, Beijing 100084, China*

Received 11 July 2012; accepted 11 July 2012
Available online 21 July 2012

**KEYWORDS**
Interface precipitation;
Dye-loading;
Light scattering

**Abstract**
A novel interface precipitation method has been developed to synthesize hierarchically structured ZnO nanocrystallite aggregates. Such synthesized ZnO nanocrystallite aggregates were demonstrated as a promising structure for high power conversion efficiency when used as photoelectrode in dye-sensitized solar cells (DSCs). In comparison with ZnO nanoparticles synthesized by conventional homogeneous precipitation method, such hierarchical structure has larger specific surface area, more efficient dye-loading and effective light scattering within the photoelectrode; all result in an increased photocurrent. Furthermore, electrochemical impedance spectroscopy study revealed that reduced charge recombination in ZnO nanocrystallite aggregates resulted in enhanced $V_{oc}$. As a result, a power conversion efficiency of 5.07% with commercially available dye N719 has been obtained without applying anti-reflection coating and chemical treatment, which was more than 200% of the power conversion efficiency achieved in ZnO nanoparticles synthesized by homogeneous precipitation method in aqueous solution.


## Introduction

Dye-sensitized solar cells (DSCs) with lower productive cost and easier fabrication are considered as alternative to the traditional silicon solar cell since they were reported first by Gratzel in 1991 [1]. Much attention had been focused on efficiency [2–7] and stability [8–13] of DSCs. Power conversion efficiency in DSCs devices based on $TiO_2$ photoanode has achieved as high as 13% using YD2-*o*-C8 dye cosensitized of Y123 dye with carefully optimized device details [14]. Photoanode is a vital component to determine the performance of DSCs, thus much study had been done on photoanode materials for DSCs. Besides of $TiO_2$, other oxide semiconductors with wide

*Corresponding author.
*E-mail addresses:* chldwang@mail.tsinghua.edu.cn (L. Wang), gzcao@u.washington.edu (G. Cao).

2211-2855/$ - see front matter © 2012 Elsevier Ltd. All rights reserved.
http://dx.doi.org/10.1016/j.nanoen.2012.07.009

bandgaps have also been studied intensively, including ZnO, $SnO_2$, $Nb_2O_5$ and so on [15–21]. Among these materials, ZnO has demonstrated to be the most promising contender, due to its similar bandgap, easier synthesis and manipulation of nano, meso, and microstructures, and its much higher electron mobility comparing to $TiO_2$ [22,23].

A lot of research has been done on the synthesis of a variety of ZnO nanostructures for efficient DSC devices. For example, as their high electron mobility, ZnO nanotubes, nanorods, and nanowires have been synthesized and studied in hope of obtaining high conversion efficiency of DSCs. However, due to small specific surface area and consequently low dye-adsorption, the devices usually showed lower conversion efficiencies than nanocrystallite DSCs [24–28]. Compared to 1-D structured photoanodes, ZnO films with hierarchical structure have exhibited much better performance in DSCs due to the larger specific surface area for dye-adsorption, effective light scattering within the photoanode, and more pores for the penetration of electrolyte into the photoanode films [29–31]. Fujihara prepared ZnO films with a rose-like morphology and used as photoanode in DSCs with a conversion efficiency of 4.1% obtained [32,33]. Zhang et al. [34] fabricated polydisperse ZnO aggregates made up of nanosized crystallites. With increased dye-adsorption and light-scattering capabilities by the primary nanoparticles and secondary colloids, 5.4% conversion efficiency was obtained [35]. Vomiero et al. used a hierarchically assembled ZnO nanocrystallites as photoanode of DSCs and obtained a 7.5% conversion efficiency with a compact buffer layer, which was the highest efficiency of ZnO DSC devices reported in open literature by now [36]. It is clear that hierarchical structure is promising for high power efficiency ZnO based DSCs.

Direct precipitation process in aqueous solution is an efficient way to synthesize ZnO with high purity and specific shapes at low temperature [37]. Compared with other routes such as electrochemical deposition, physical/chemical vapor deposition or hydrothermal methods, this method features simpler operation and lower cost, and is more ideal for industrial production.

In this paper, a novel interface precipitation method has been developed to synthesize hierarchically structured ZnO nanocrystallite aggregates [35]. Ethanol and water were used as solvents to first separately dissolve NaOH and zinc acetate dihydrate under stirring, respectively. The reaction occurred in the interface of the different solvents with a slow rate, which was easier to form a porous hierarchical structure. As a result, porous ZnO nanocrystallite aggregates were obtained. The aggregates consisted of loosely packed primary nanocrystallites and possess irregular shape with size distribution ranging from ~100 nm to ~1 μm. Such fabricated ZnO nanocrystallite aggregates differ markedly from the ZnO aggregates synthesized by hydrothermal method [31,35]. The initial characterization and performance test revealed that such synthesized ZnO nanocrystallite aggregates are very promising structure for high power conversion efficiency when used to fabricate photoelectrode for DSCs. Compared to ZnO nanoparticles synthesized by homogeneous precipitation method in aqueous system, this structure had larger specific surface area, better dye-loading and light scattering; all increased photocurrent effectively. Furthermore, electrochemical impedance spectroscopy study revealed reduced charge recombination, leading to much enhanced $V_{oc}$. A power conversion efficiency of 5.07% under illumination of 100 mW/cm$^2$ has obtained with the annealing temperature of 300 °C, which was much higher than using ZnO nanoparticles synthesized by homogeneous precipitation method in aqueous solution.

## Experimental procedure

### Synthesis of hierarchically ZnO nanocrystallites and fabrication of photoanode

Hierarchically assembled ZnO nanocrystallites aggregates were synthesized through a novel interface precipitation method. First, 3.6 g zinc acetate dihydrate was added to distilled water (20 mL) and 1.6 g NaOH was dissolved in ethanol (500 mL) at 60 °C. Then poured the solution of zinc acetate dehydrate in to the NaOH–ethanol solution and with strong stirring meanwhile. One hour later, the as-obtained colloidal solution was then sequentially concentrated by centrifugally separating the ZnO from the solvent and then dispersed the precipitate in ethanol (3 mL). The doctor-blade technique was used to prepare porous ZnO layer on an FTO glass substrate and the thickness was controlled by a tape.

### Assembly of the DSCs devices

The ZnO photoanode was sintered at 300 °C, then immersed in 0.3 mM N719 absolute ethanol solution for 60 min, followed by cleaning with absolute ethanol. This time was optimized in the earlier work to prevents the over sufficient dye-loading and limits the power conversion efficiency [38]. The electrolyte in this study was a liquid admixture containing 0.5 M tetrabutylammonium iodide, 0.1 M lithium iodide, 0.1 M iodine, and 0.5 M 4-*tert*-butylpyridine in acetonitrile. A chemically platinized silicon wafer was used as the counter electrode. When assembling the DSC, the electrolyte was sandwiched by a sensitized ZnO electrode and a counter electrode with two clips.

### Characterization

The morphology and surface area of the as-synthesized ZnO nanocrystallites were characterized by scanning electron microscopy (SEM, JEOL JSM-7000) and Brunauer–Emmett–Teller (BET, Quantachrome NOVA 4200e). X-Ray Diffraction (Philips PW1830 Diffractometer) and JADE software (MDI JADE 7 Materials Data XRD Pattern Processing, Identification, and Quantification) were used to verify the phase and crystal structure of the ZnO films. Optical absorption (Perkin Elmer Lambda 900 UV/VIS/IR Spectrometer) was used to analyze the diffuse reflectance and diffuse transmittance of the ZnO films. The photovoltaic behavior was characterized when the cell devices were irradiated by simulated AM 1.5 sunlight with an output power of 100 mW/cm$^2$. An Ultraviolet Solar Simulator (model 16 S, Solar Light Co., Philadelphia, PA) with a 200 W Xenon Lamp Power Supply (Model XPS 200, Solar Light Co., Philadelphia,PA) was used as the light source, and a Semiconductor Parameter Analyzer (4155 A, Hewlett–Packard, Japan) was used to measure

the current and voltage. The electrochemical impedance spectroscopy (EIS) was carried out through the Solartron 1287 A coupling with the Solartron 1260 FRA/impedance analyzer to investigate electronic and ionic processes in DSCs. The film thickness was investigated by Veeco Dektak 6M Stylus Profilometer.

## Results and discussion

Figure 1 compares the SEM images of ZnO nanoparticle films (a) and (c) synthesized with homogeneous precipitation method using aqueous system and ZnO nanocrystallite aggregates films (b) and (d) through interface precipitation method. ZnO

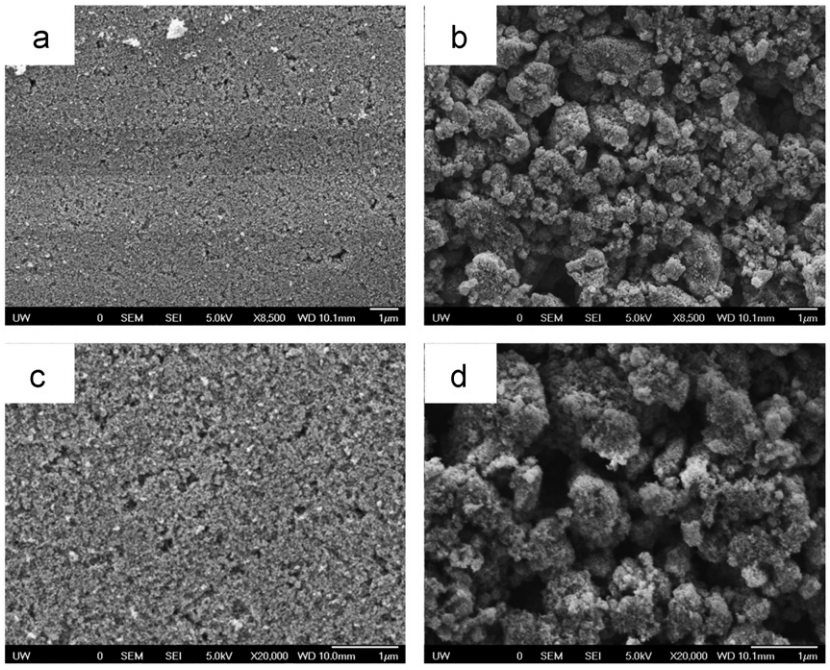


**Figure 1** (a) and (c) SEM images of ZnO synthesized through homogeneous precipitation method using aqueous system and (b) and (d) interface precipitation method in different magnification.

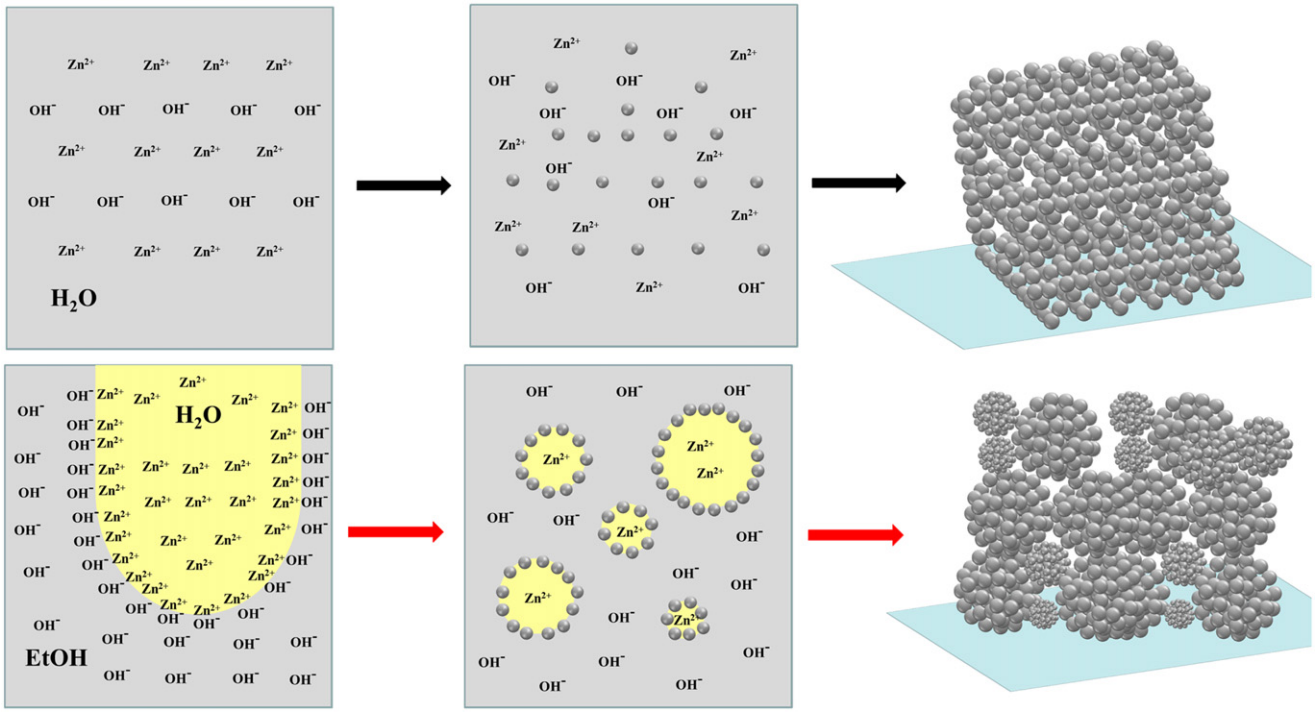


**Scheme 1** Schematic diagram of ZnO formation process using homogeneous (top) and interface precipitation methods (bottom).

nanoparticles are typically 10 to ~20 nm in diameter, and the film is compact with a few voids. While, the ZnO nanocrystallite aggregates possess a size ranging from ~100 nm to ~1 μm in diameter, and the nanocrystallites assembled in aggregates were also about ~10 to ~20 nm. The ZnO nanocrystallite aggregates film was much more porous with voids as large as several micrometers. Such appreciably different nano/microstructures are ascribed to the different precipitation methods used in this study Scheme 1 depicts and illustrate the differences. In aqueous system, the $Zn^{2+}$ and $OH^{-}$ reacted with each other uniformly in the bulk of the solution. When the concentration is low, after initial nucleation, no secondary nucleation is expected and the nanoparticles would grow by attracting the remaining $Zn^{2+}$ and $OH^{-}$ ions from the surrounding vicinity till their depletion. Uniformly sized single crystalline nanoparticles are formed as anticipated, and uniform compact films with little voids can be readily fabricated shown in Figure 1(a) and (c). However, when the interface precipitation method was applied, the chemical reaction and initial nucleation would take place at the interface of water and ethanol only, as the reaction rate is far higher than the diffusion rate of ethanol in water [39]. The subsequent nanocrystallite growth take places as more zinc cations and hydroxyl anions are brought to the interface as a result of counter diffusion and mixing of ethanol and water. Assuming initially water droplets disperse in ethanol, the nucleation and subsequent growth occur at the interface and the water diffuses out to mix with ethanol (water has higher diffusivity than ethnol) [40], resulting in a recession of perimeter of the water droplets and eventually leading to the formation of hierarchically structured ZnO, i.e., micrometer sized aggregates of ZnO nanocrystals, as shown in Figure 1(b) and (d).

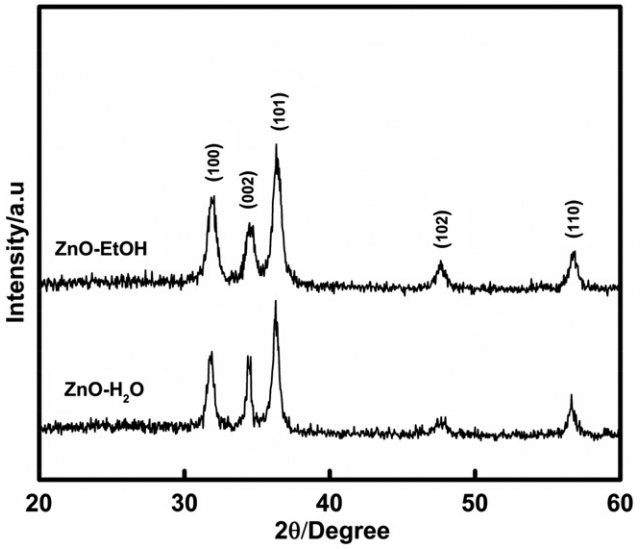


**Figure 2** XRD spectra of ZnO synthesized through different precipitation methods.

Figure 2 are the XRD patterns of ZnO nanocrystals and nanocrystallite aggregrates; the XRD peaks can very well indexed to ZnO regardless the different precipitation methods (Joint Committee on Powder Diffraction Standards—JCPDS card number 36-1451). Using the Scherer equation, the size of nanocrystals synthesized through homogeneous and interface precipitation methods were estimated to be about 20.7 nm and 17.7 nm. This result is consistent with the SEM images. The smaller size of nanocrystals would be expected to possess larger specific surface area.Thus nitrogen sorption isotherms were used to characterize the specific surface area, pore size and porosity of individually dispersed ZnO nanocrystallites and aggregated ZnO nanocrystallites.

Figure 3 shows the nitrogen sorption isotherms (a) and pore size distribution (b). The isotherms for both materials showed a type IV pattern with a sharp increase in nitrogen volume adsorbed at a high relative pressure ($P/P_0$=0.65-0.95), indicating the nature of mesoporous [41]. The ZnO nanocrystals synthesized through homogeneous precipitation in water would be solid; the mesopores are likely the voids between packed nanoparticles. However, the aggregates formed through interface precipitation are porous with pores. As shown in Figure 3(b), the mean pore diameter between nanoparticles of ZnO synthesized through homogeneous precipitation was found to 27 nm, larger than 18 nm in the ZnO nanocrystallite aggregates through interface precipitation. In addition, the pores between ZnO nanoparticles have broader size distribution, while the pore size in ZnO nanocrystallite aggregates is narrowly distributed. The above BET results revealed the nanocrystallites in the aggregates were packed more closely. As shown in the SEM images, the pores between the aggregates were larger than 200 nm, which is beyond the BET detection limit. The

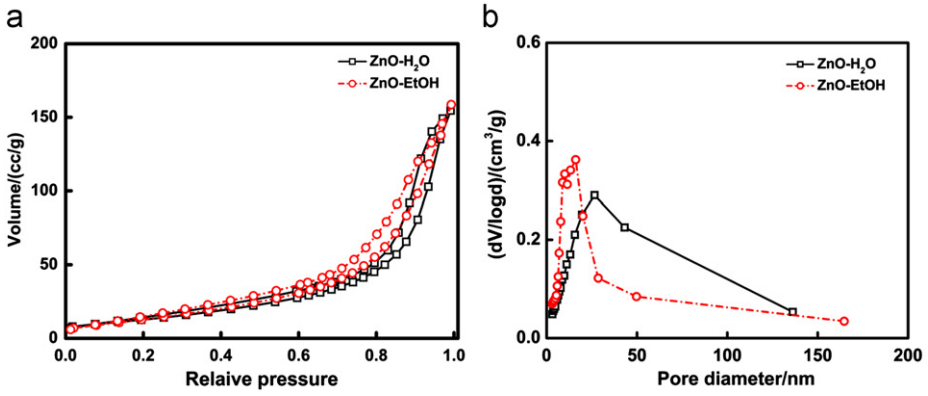


**Figure 3** (a) Nitrogen sorption isotherms and (b) pore size distributions of ZnO synthesized through different precipitation methods.

results from nitrogen sorption isotherms calculated using BET method are summarized in Table 1. As shown in Table 1, the film thickness of ZnO synthesized through different precipitation methods was comparative, which were 15.02 and 15.87 μm, respectively. The specific surface area of ZnO nanoparticles synthesized through homogeneous precipitation method was 60 $m^2/g$, and that of ZnO aggregates was 84 $m^2/g$, respectively. The latter was about 40% larger than former. It could be easily ascribed to the smaller size of nanocrystallites in the aggregates.The BET results corroborate well with the crystallite size calculted from XRD patterns using Scherer equation. The amounts of dye molecules loaded per unit area of photoelectrode and per unit specific surface area were measured and calaculated. The dye-loading of ZnO nanocrystallite aggregates synthesized by interface precipitation was $2.29 \times 10^{-7}$ mol/$cm^2$, and that of homogeneous nanoparticles was $1.38 \times 10^{-7}$ mol/$cm^2$, respectively. The much larger amount of dye loaded per unit area of photoelectrodes made of ZnO nanocrystallite aggregates might be due to the larger specific surface area as compared to that of ZnO nanoparticles. Further analysis revealed that the amount of dyes loaded per specific surface area of ZnO nanocrystallite aggregates synthesized by interface precipitation was $9.05 \times 10^{-7}$ mol/$m^2$, which was much larger than that of ZnO nanoparticles, $5.56 \times 10^{-7}$ mol/$m^2$. The results strongly suggest the surface properties of ZnO nanocrystallite aggregates and ZnO nanoparticles are appreciably different and ZnO aggregates showes much better surface chemistry for dye-loading. It is not known to us at the moment what are the cause for such a difference, though possible explanations include (1) the nanocrystallites are predominated with different facets, (2) different dangling bonds on the surface, and (3) surface contamination. More work is underway to characterize the surface properties.

**Table1** Summary of the film properties of ZnO synthesized by different precipitation methods.

| | ZnO-EtOH | ZnO-$H_2O$ |
|---|---|---|
| Film thickness (μm) | 15.02 | 15.87 |
| Surface area ($m^2/g$) | 84 | 60 |
| Pore volume (mL/g) | 0.253 | 0.242 |
| Pore diameter (nm) | 16 | 27 |
| Dye-loading ($10^{-7}$ mol/$cm^2$) | 2.29 | 1.38 |
| Dye-loading per specific area($10^{-7}$ mol/$m^2$) | 9.05 | 5.56 |

To increase the probability of absorbing incident photons, efficient light scattering is necessary for highly performed photoanodes of DSCs. Thus light-scattering was important property of photoanode that influence the performance of DSCs. In this paper, light scattering characterization of the samples without sensitization were carried out in a UV-vis spectrophotometer equipped with an integrating sphere. Diffuse reflectance and transmission can reveal the extent that the incident light is scattered by particles in the photoanode and how much incident light passes through the photoanode without being scattered. The ideal light scattering activities of the photoanode should have a higher diffuse reflectance and lower diffuse transmittance [25-27]. As shown in Figure 4 (a), the diffuse reflectance of ZnO aggregates was much stronger in the range of 400-800 nm, which was the main wavelength range dye used in DSCs could capture the photons effectively. Figure 4(b) showed that the diffuse transmittance of ZnO aggregates was weaker than that of nanoparticles, showing stronger effect

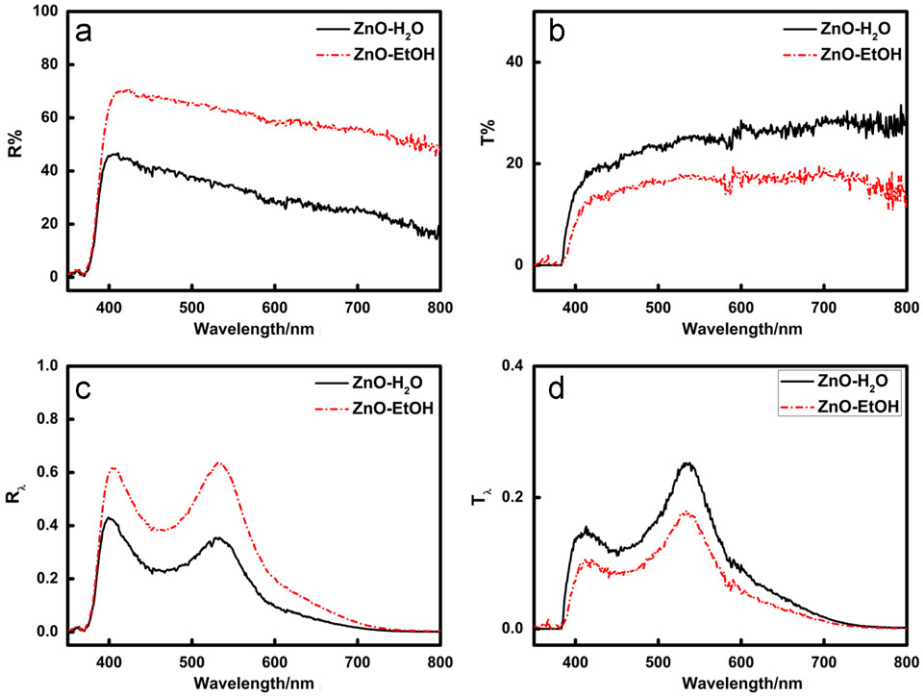


**Figure 4** (a) Diffuse reflectance, (b) diffuse transmittance, (c) relative diffuse reflectance, (d) relative diffuse transmittance spectra of ZnO films without sensitization synthesized by different precipitation methods.

to trap the photons in the photoanode film. As a result, incident light could be scattered more efficiently by the ZnO aggregates synthesized by interface precipitation method. Then the photocurrent of devices based on ZnO aggregates could be increased by the enhanced light scattering.

As only the light scattering in the range that dye used in the device could absorb was benificial to enhance the light capture, here new parameters and named them as ''relative diffuse reflectance'' and ''relative diffuse transmittance'' ($R_r$ and $T_r$) were proposed to furhter investigating the light scattering effects of different ZnO structured photoanode. The $R_r$ and $T_r$ in the range from $\lambda_1$ to $\lambda_2$ can be calculated from the measured diffuse reflectance and diffuse transmittance using the formula, given as followed equations [42]:

$$R_r = \frac{\int_{\lambda_1}^{\lambda_2} I_\lambda R_\lambda d\lambda}{\int_{\lambda_1}^{\lambda_2} I_\lambda d\lambda} \quad (1)$$

$$T_r = \frac{\int_{\lambda_1}^{\lambda_2} I_\lambda T_\lambda d\lambda}{\int_{\lambda_1}^{\lambda_2} I_\lambda d\lambda} \quad (2)$$

where $R_\lambda$ and $T_\lambda$ are diffuse reflectance and diffuse transmittance at the certain wavelength, which were measured in Figure 4(a) and (b). $I_\lambda$ is the normalized absorption spectra intensity of N719 dye at $\lambda$ wavelength, the $\lambda_1$-$\lambda_2$ is corresponding to 350-800 nm in this work. The results shown in Figure 4(c) and (d) indicated that ZnO aggregates synthesized by interface precipitation method showed higher diffuse reflectance and lower diffuse transmittance than ZnO nanoparticles in the range that N719 dye absorbed effectively, which accorded with the results in Figure 4(a) and (b). Furthermore, as calculated from Eq. (1), the relative diffuse reflectance of ZnO aggregates and nanoparticles were 0.556 and 0.325 , respectively, the former was much higher than that of the latter. The results indicated that in the range of spectra which dye could absorb effectively, the ZnO aggregates synthesized by interface precipitation method performed better light scattering than nanoparticles synthesized by homogeneous precipitation method. Smilarly, as calculated from Eq. (2), the relative diffuse transmittance of ZnO aggregates and nanoparticles were 0.130 and 0.190, the former was lower than that of the latter. The results further indicated that in the range of spectra which dye could absorb effectively, the ZnO aggregates synthesized by interface precipitation method performed better light scattering, which could increase the photocurrent.

As shown in Figure 5(a) and Table 2, compared to the ZnO nanoparticles synthesized by homogeneous precipitation method, the short-circuit current density ($J_{sc}$) of devices based on the ZnO aggregates synthesized by interface precipitation method increased from 6.90 mA/cm$^2$ to 11.41 mA/cm$^2$, with a 65.2% increasing relatively. As discussed above, the significantly increased photocurrent was due to the larger surface area for dye-loading, more porous, and stronger light scattering, which were shown in the results of SEM, BET and diffuse reflectance and transmittance spectra shown in Figures 1, 3, 4 and Table 1. Besides of $J_{sc}$, the open-circuit voltage ($V_{oc}$) and fill factor (FF) of DSCs device based on ZnO aggregates also were higher comparing with the devices based on nanoparticles. As shown in Table 2, the $V_{oc}$ enhanced from 0.54 V to 0.64 V, and the FF increased from 0.57 to 0.69, both showing obvious improvement. As a result, the conversion efficiency of device based on ZnO aggregates synthesized by interface precipitation method increased from 2.12% to 5.07% under AM 1.5, 100 mW/cm$^2$ illumination with a 139% relative enhancement, showing a much better performance than device based on ZnO nanoparticles synthesized by homogeneous precipitation method. Compared to the earilier literature that obtained high conversion efficiency, [19,29] our work also really had some advantages, such as simple synthesis, lower power spending as lower synthesizing and annealing temperature. Regarding the specific conversion efficiency of 5% obtained by Hagfeldt and co-workers, [19] this high efficiency was tested under 100 W/m$^2$ (or 10 mW/cm$^2$) illumination, which was 10 times weaker than the one sun illumination commonly used and reported in literatures. It is well known that DCSs will show a much higher power efficiency when the illumination was lower as there will be much less charge recombination due to a lower density of electrons generated by a low photon intensity. More detailed experimental results and discussion can be found in Ref 36. In addition, Hagfeldt and co-workers also used a pressure of 1000 kg/cm$^2$ to improve the contact of film and glass, which was much more difficult than the method we used. Efficiency larger than 6% were obtained more recently by Fujihara et al.

**Table 2** Photo-voltaic parameters of devices based on ZnO synthesized by different precipitation methods.

| | $V_{oc}$ (V) | $J_{sc}$ (mA/cm$^2$) | FF | $\eta$% |
|---|---|---|---|---|
| ZnO-EtOH | 0.64 | 11.41 | 0.69 | 5.07 |
| ZnO-$H_2O$ | 0.54 | 6.90 | 0.57 | 2.12 |

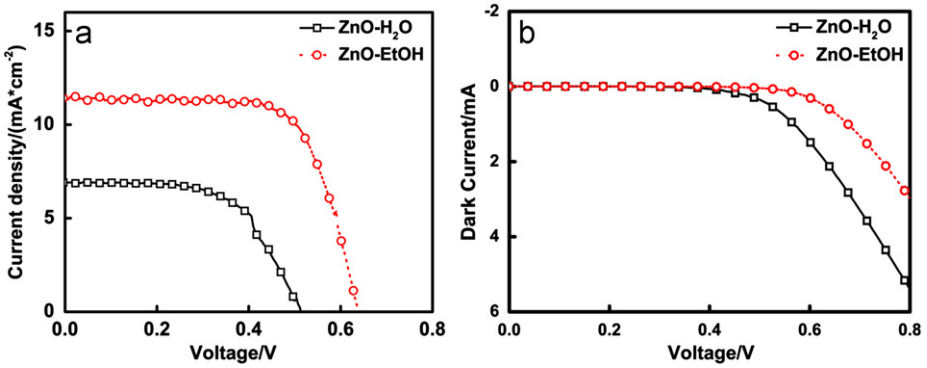


**Figure 5** *I-V* curves of devices based on ZnO synthesized by different precipitation methods uner illumination (a) and in dark (b).

[29]. Such efficiency was achieved through some systematic device optimization. A power conversion efficiency of 4.14% was achieved before optimization. Fujihara's paper demonstrated that the optimization of device fabrication has a significant impact on the power conversion efficiency. The focus of our work was on ZnO aggregates through new synthesis method and demonstrated that such synthesized aggregates promised much higher power conversion efficiency of 5% as compared to 2% with the ZnO photoanode with homogeneous precipitation method. With further optimization of device fabrication, much higher power conversion efficiency might be achieved. Compared to the samples in the above mentioned literatures, the larger amount of dye-loading was due to the larger specific surface area; however, and the lower photocurrent could be due to more charge recombination associated with our lower annealing temperature. In Refs. [29,36] the annealing temperatures used were both 450 °C, which is much higher than 300 °C that we used. The higher annealing temperature could improve the connection between adjacent ZnO nanoparticles and subsequently benefit the electron transport, which could cause the enhancement of photocurrent. However, higher annealing temperature meant spending much more power to fabricate the devices, which could limit the application of DSCs. In Ref. 36, the enhancement of photocurrent is mainly due to the use of a buffer layer, which is not used in our work. Without a buffer layer, the photocurrent was 7.5 mA/cm$^2$ and the efficiency was 2.6%. With a buffer layer but annealed at 370 °C, they got 4.9% efficiency, which well supports our results and explanations. As shown in Figure 5(b), the dark current of device based on ZnO aggregates decreased compared to that based on ZnO nanoparticles, indicating a lower charge recombination from the conduction band of ZnO to the redox couple in the electrolyte.

To further understand the charge transfer property in the DSC devices based on ZnO synthesized by different precipitation methods, the EIS analyses were carried out. Charge recombination influenced the $V_{oc}$ and conversion efficiency effectively. As DSC could be considered as a leaking capacitor in dark condition [43], the resistance of the back reaction from $TiO_2$ to the triiodide ions in the electrolyte was analyzed through EIS under dark condition with a bias voltage of −0.7 V. DSC could be interpreted using only resistance-capacitance (*RC*) elements in an equivalent circuit [44], as inserted in Figure 6(a). The impedance associated with the charge transfer process occurring at Pt electrode/electrolyte interface is determined, which is characterized by the charge transfer resistance ($R_1$) and the capacitance ($CPE_1$). In the middle frequency range $10^3$-1 Hz, the impedance related to the charge transfer process at the $TiO_2$/dye/electrolyte interface can be described by $R_2$ and the $CPE_2$. And in the low frequency 0.1-10 Hz, the Warburg diffusion impedance ($Z_w$) within the electrolyte will be estimated. We mainly focused on the $R_2$ and $CPE_2$ which represented the charge transfer process at the $TiO_2$/dye/electrolyte interface. A larger value of $R_2$ meant less charge recombination at the sensitized ZnO/electrolyte interface [45]. As shown in Figure 6(a) and Table 3, comparing to ZnO nanoparticles, the ZnO aggregates synthesized by interface precipitation method had a much larger value of $R_2$, which represented the charge recombination from the conduction band of ZnO to the redox couple in the electrolyte. This result showed that electrons in photoanode of ZnO aggregates were more difficult to recombination, which accorded with the result of dark current curves shown in Figure 6(b).

Bode plots of devices based on ZnO synthesized by different precipitation methods were shown in Figure 6(b). The three peaks in the phase of the spectrum were associated with three transient processes in the DSC. The middle-frequency peak (in the 10-100 Hz range) was determined by the lifetime of the electrons in the ZnO, which was shown as follow equation [46]:

$$\tau = \frac{1}{2\pi f_{peak}} \tag{3}$$

As shown in Figure 6(b), the frequency at minimum phase angle peak of device based on ZnO aggregates synthesized by interface precipitation method was smaller than that based on ZnO nanoparticles. As a result, from Eq. (3), the

**Table 3** Resistances of devices based on ZnO synthesized by different precipitation methods.

| | $R_1$ | $R_2$ | $Z_d$ |
|---|---|---|---|
| ZnO-EtOH | 10.7 | 62.8 | 21.5 |
| ZnO-$H_2O$ | 7.3 | 32.2 | 40.7 |

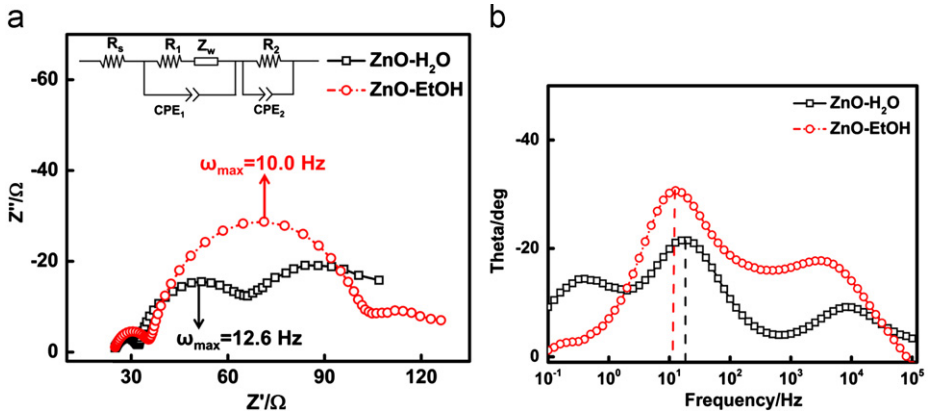


**Figure 6** (a) Nyquist plot and (b) Bode plot of devices based on ZnO synthesized by different precipitation methods under dark condition.

lifetime of electrons in the conduction band was enhanced by using ZnO aggregates.

The $V_{oc}$ of DSCs could be expressed by follow equation [47]:

$$V_{oc} = \frac{RT}{\beta F} \ln\left(\frac{AI}{n_0 k_b [I_3^-] + n_0 k_r [D^+]}\right) \quad (4)$$

where $R$ is the molar gas constant, $T$ is the temperature in Kelvin, $F$ is the Faraday constant, $\beta$ is the reaction order for $I_3^-$ and electrons, $A$ is the electrode area, $I$ is the incident photon flux, $n_0$ is the concentration of accessible electronic states in the conduction band and $k_b$ and $k_r$ are the kinetic constant of the back reaction of the injected electrons with triiodide and the recombination of these electrons with oxidized dyes, respectively. It could be considered that frequency at themaximum imaginary resistance of the Nyquist plot ($\omega_{max}$) was the same as the back reaction constant ($k_b$).[47,48] The value of $V_{oc}$ increased with the decreasing of back reaction constant, which was as same as $\omega_{max}$. As shown in Figure 6(a), the $\omega_{max}$ value of device based on ZnO aggregates was smller than that based on ZnO nano particles. From Eq. (4), the $V_{oc}$ of device based on ZnO aggregates could increase compared to that based on ZnO nanoparticles, which accorded with the measured results of *I-V* curves shown in Figure 5(a). The $k_b$ also could be calculated from the following equation [49]:

$$k_b = \frac{1}{(R_2 Q_2)^{1/n_2}} \quad (5)$$

where $Q_2$ is the *CPE* prefactor and $n_2$ is the CPE index. Eq. (5) also indicated that a larger $R_2$ meant a smaller $k_b$, resulting in a higher $V_{oc}$ from Eq. (4). As discussed above, ZnO aggregates synthesized by interface precipitation method showed a lower charge recombination and longer electron lifetime in the conduction band than ZnO nanoparticles synthesized by homogeneous precipitation method, which could enhance the $V_{oc}$ and conversion efficiency of DSCs devices.

## Conclusions

A novel interface precipitation method has been developed to synthesize hierarchically structured ZnO nanocrystallite aggregates. The aggregates consist of loosely packed primary nanocrystallites and possess irregular shape with size distribution ranging from ~100 nm to ~1 μm. Such synthesized ZnO nanocrystallite aggregates are very promising structure for high power conversion efficiency when used to fabricate photoelectrode for DSCs. Compared to ZnO nanoparticles synthesized by homogeneous precipitation method, this structure had larger surface area, better dye-loading and light scattering, which contribute to a significantly increased photocurrent. In addition, EIS analysis suggested interface precipitated ZnO nanocrystallite aggregates have less charge recombination, which could enhance $V_{oc}$. As a result, a power conversion efficiency of 5.07% under illumination of 100 mW/cm$^2$ has obtained, which was much higher than that based on ZnO nanoparticles synthesized by homogeneous precipitation method in aqueous solution. With a little optimization of the interface precipitation process and device fabrication, further enhancement in power conversion efficiency is expected.

## Acknowledgements

This work has been supported in part by the US Department of Energy, Office of Basic Energy Sciences, Division of Materials and Engineering under Award No. DE-FG02-07ER46467 (Q.F.Z.) on the microstructure characterization and some power conversion efficiency measurements, National Science Foundation (DMR-1035196), the National Natural Science Foundation of China under Grant No. 50873055 and the National Key Basic Research and Development Program of China under Grant No. 2009CB930602. R. Gao would also like to thank the China Scholarship Council (CSC) for providing scholarship for Ph.D. study at the University of Washington.

## References

[1] B. Oregan, M. Gratzel, Nature 353 (1991) 737–740.
[2] D. Kuang, C. Klein, S. Ito, J.-E. Moser, R. Humphry-Baker, S.M. Zakeeruddin, M. Graetzel, Advanced Functional Materials 17 (2007) 154–160.
[3] L. Hu, S. Dai, J. Weng, S. Xiao, Y. Sui, Y. Huang, S. Chen, F. Kong, X. Pan, L. Liang, K. Wang, Journal of Physical Chemistry B 111 (2007) 358–362.
[4] R. Gao, L. Wang, B. Ma, C. Zhan, Y. Qiu, Langmuir 26 (2010) 2460–2465.
[5] R. Gao, B.B. Ma, L.D. Wang, Y.T. Shi, H.P. Dong, Y. Qiu, Acta Physico-Chimica Sinica 27 (2011) 413–418.
[6] R. Gao, L. Wang, Y. Geng, B. Ma, Y. Zhu, H. Dong, Y. Qiu, Physical Chemistry Chemical Physics 13 (2011) 10635–10640.
[7] R. Gao, L. Wang, Y. Geng, B. Ma, Y. Zhu, H. Dong, Y. Qiu, Journal of Physical Chemistry C 115 (2011) 17986–17992.
[8] Q.B. Meng, K. Takahashi, X.T. Zhang, I. Sutanto, T.N. Rao, O. Sato, A. Fujishima, H. Watanabe, T. Nakamori, M. Uragami, Langmuir 19 (2003) 3572–3574.
[9] E. Figgemeier, A. Hagfeldt, International Journal of Photoenergy 6 (2004) 127–140.
[10] P.M. Sommeling, M. Spath, H.J.P. Smit, N.J. Bakker, J.M. Kroon, Journal of Photochemistry and Photobiology A—Chemistry 164 (2004) 137–144.
[11] S. Nakade, T. Kanzaki, S. Kambe, Y.J. Wada, S. Yanagida, Langmuir 21 (2005) 11414–11417.
[12] M. Gratzel, Comptes Rendus Chimie 9 (2006) 578–583.
[13] A.R.S. Priya, A. Subramania, Y.S. Jung, K.J. Kim, Langmuir 24 (2008) 9816–9819.
[14] A. Yella, H.W. Lee, H.N. Tsao, C.Y. Yi, A.K. Chandiran, Science 334 (2011) 629–633.
[15] M. Matsumura, S. Matsudaira, H. Tsubomura, M. Takata, H. Yanagida, Industrial & Engineering Chemistry Product Research and Development 19 (1980) 415–421.
[16] G. Redmond, D. Fitzmaurice, M. Graetzel, Chemistry of Materials 6 (1994) 686–691.
[17] H. Rensmo, K. Keis, H. Lindstrom, S. Sodergren, A. Solbrand, A. Hagfeldt, S.E. Lindquist, L.N. Wang, M. Muhammed, Journal of Physical Chemistry B 101 (1997) 2598–2601.
[18] K. Sayama, H. Sugihara, H. Arakawa, Chemistry of Materials 10 (1998) 3825–3832.
[19] K. Keis, E. Magnusson, H. Lindstrom, S.E. Lindquist, A. Hagfeldt, Solar Energy Materials and Solar Cells 73 (2002) 51–58.
[20] T. Stergiopoulos, I.M. Arabatzis, H. Cachet, P. Falaras, Journal of Photochemistry and Photobiology A—Chemistry 155 (2003) 163–170.
[21] N.G. Park, M.G. Kang, K.S. Ryu, K.M. Kim, S.H. Chang, Journal of Photochemistry and Photobiology A—Chemistry 161 (2004) 105–110.
[22] Q. Zhang, G. Cao, Nano Today 6 (2011) 91–109.
[23] Q. Zhang, C.S. Dandeneau, X. Zhou, G. Cao, Advanced Materials 21 (2009) 4087–4108.
[24] D.I. Suh, S.Y. Lee, T.H. Kim, J.M. Chun, E.K. Suh, O.B. Yang, S.K. Lee, Chemical Physics Letters 442 (2007) 348–353.

[25] E. Galoppini, J. Rochford, H. Chen, G. Saraf, Y. Lu, A. Hagfeldt, G. Boschloo, Journal of Physical Chemistry B 110 (2006) 16159–16161.
[26] J.B. Baxter, E.S. Aydil, Solar Energy Materials and Solar Cells 90 (2006) 607–622.
[27] M. Law, L.E. Greene, J.C. Johnson, R. Saykally, P.D. Yang, Nature Materials 4 (2005) 455–459.
[28] M. Guo, P. Diao, X.D. Wang, S.M. Cai, Journal of Solid State Chemistry 178 (2005) 3210–3215.
[29] M. Saito, S. Fujihara, Energy & Environmental Science 1 (2008) 280–283.
[30] C.-H. Ku, J.-J. Wu, Applied Physics Letters 91 (2007).
[31] T.P. Chou, Q. Zhang, G.E. Fryxell, G. Cao, Advanced Materials 19 (2007) 2588–2592.
[32] K. Kakiuchi, E. Hosono, S. Fujihara, Journal of Photochemistry and Photobiology A—Chemistry 179 (2006) 81–86.
[33] E. Hosono, S. Fujihara, T. Kimura, Electrochimica Acta 49 (2004) 2287–2293.
[34] Q. Zhang, T.P. Chou, B. Russo, S.A. Jenekhe, G. Cao, Advanced Functional Materials 18 (2008) 1654–1660.
[35] Q. Zhang, T.R. Chou, B. Russo, S.A. Jenekhe, G. Cao, Angewandte Chemie—International Edition 47 (2008) 2402–2406.
[36] N. Memarian, I. Concina, A. Braga, S.M. Rozati, A. Vomiero, G. Sberveglieri, Angewandte Chemie—International Edition 50 (2011) 12321–12325.
[37] Y. Shi, C. Zhan, L. Wang, B. Ma, R. Gao, Y. Zhu, Y. Qiu, Advanced Functional Materials 20 (2010) 437–444.
[38] T.P. Chou, Q. Zhang, G. Cao, Journal of Physical Chemistry C 111 (2007) 18804–18811.
[39] E.M. Wong, J.E. Bonevich, P.C. Searson, Journal of Physical Chemistry B 102 (1998) 7770–7775.
[40] K.C. Pratt, W.A. Wakeham, Proceedings of the Royal Society A: Mathematical, Physical and Engineering Sciences 336 (1974) 393–406.
[41] F. Huang, D. Chen, X.L. Zhang, R.A. Caruso, Y.-B. Cheng, Advanced Functional Materials 20 (2010) 1301–1305.
[42] Z. Liang, Q. Zhang, O. Wiranwetchayan, J. Xi, Z. Yang, K. Park, C. Li, G. Cao, Advanced Functional Materials 22 (2012) 2194–2201.
[43] J. Bisquert, Journal of Physical Chemistry B 106 (2002) 325–333.
[44] Q. Wang, J.E. Moser, M. Gratzel, Journal of Physical Chemistry B 109 (2005) 14945–14953.
[45] Z. Huo, S. Dai, K. Wang, F. Kong, C. Zhang, X. Pan, X. Fang, Solar Energy Materials and Solar Cells 91 (2007) 1959–1965.
[46] R. Kern, R. Sastrawan, J. Ferber, R. Stangl, J. Luther, Electrochimica Acta 47 (2002) 4213–4225.
[47] K. Lee, S.W. Park, M.J. Ko, K. Kim, N.-G. Park, Nature Materials 8 (2009) 665–671.
[48] M. Adachi, M. Sakamoto, J. Jiu, Y. Ogata, S. Isoda, Journal of Physical Chemistry B 110 (2006) 13872–13880.
[49] F. Fabregat-Santiago, G. Garcia-Belmonte, I. Mora-Sero, J. Bisquert, Physical Chemistry Chemical Physics 13 (2011) 9083–9118.

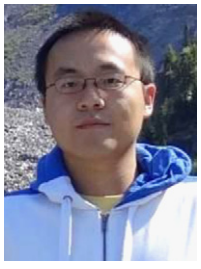

**Rui Gao** is pursuing Ph.D. in Department of Chemistry at Tsinghua University, Beijing and now works as a visiting student in Department of Materials Science, University of Washington. His current research is focused on the interface modification and photoanode material synthesis of dye-sensitized solar cells.

**Zhiqiang Liang** is pursuing Ph.D. in the School of Material Science and Engineering, Harbin Institute of Technology and worked as a visiting student in Department of Materials Science, University of Washington. His current research is focused on the inverted polymer solar cells.

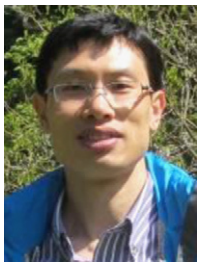

**Jianjun Tian** is working as an associate professor in Advanced Material and Technology Institute, University of Science and Technology Beijing and now works as a visiting scholar in Department of Materials Science, University of Washington. His current research is focused on quantum dot sensitized solar cells.

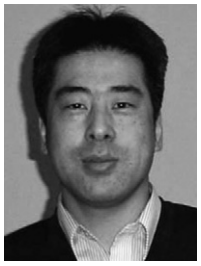

**Qifeng Zhang** is currently working at University of Washington as a Research Assistant Professor. His research interests involve engineering applications of nano-structured materials on electrical devices including solar cells, UV light-emitting diodes (LEDs), ?eld-effect transistors (FETs), and gas sensors. His current research focuses on the synthesis of nanomaterials and the application of nanomaterials in electronic and optoelectronic devices, such as dye-sensitized solar cells (DSCs) and organic/inorganic hybrid solar cells.

**Liduo Wang** is a professor in Department of Chemistry at Tsinghua University, Beijing. His recent research is focused mainly on solar cells, organic light-emitting diode (OLED) and organic thin film transistor (OTFT).

**Guozhong Cao** is a Boeing Steiner Professor of Materials Science and Engineering, Professor of Chemical Engineering, and Adjunct Professor of Mechanical Engineering at the University of Washington. He has published over 280 papers, 7 books and 4 proceedings. His recent research is focused mainly on solar cells, lithium-ion batteries, supercapacitors, and hydrogen storage.